

AL-TR-1991-0103

AD-A248 290



**SIMULATION IN INFRARED IMAGING: USING
ELECTRICAL CIRCUIT PRINCIPLES TO
MODEL HEAT TRANSFER**

Ronald J. Evans

**University of Dayton Research Institute
300 College Park Avenue
Dayton, OH 45469**

**DTIC
SELECTED
APR 2 1992
S B D**

**HUMAN RESOURCES DIRECTORATE
AIRCREW TRAINING RESEARCH DIVISION
Williams Air Force Base, AZ 85240-6457**

January 1992

Final Technical Report for Period May 1990 - August 1991

Approved for public release; distribution is unlimited.

92-08301



**AIR FORCE SYSTEMS COMMAND
BROOKS AIR FORCE BASE, TEXAS 78235-5000**

ARMSTRONG


LABORATORY

NOTICES

When Government drawings, specifications, or other data are used for any ~~purpose other than~~ in connection with a definitely Government-related procurement, the United States Government incurs ~~no responsibility~~ or any obligation whatsoever. The fact that the Government may have formulated or in any way supplied the said drawings, specifications, or other data, is not to be regarded by implication, or otherwise in any manner construed, as licensing the holder, or any other person or corporation; or as conveying any rights or permission to manufacture, use, or sell any patented invention that may in any way be related thereto.

The Office of Public Affairs reviewed this report, and it is releasable to the National Technical Information Service, where it will be available to the general public, including foreign nationals.

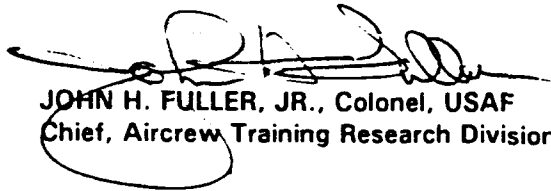
This report has been reviewed and is approved for publication.



BYRON J. PIERCE
Project Scientist



DEE H. ANDREWS, Technical Director
Aircrew Training Research Division



JOHN H. FULLER, JR., Colonel, USAF
Chief, Aircrew Training Research Division

REPORT DOCUMENTATION PAGEForm Approved
OMB No. 0704-0188

Public reporting burden for this collection of information is estimated to average 1 hour per response, including the time for reviewing instructions, searching existing data sources, gathering and maintaining the data needed, and completing and reviewing the collection of information. Send comments regarding this burden estimate or any other aspect of this collection of information, including suggestions for reducing this burden, to Washington Headquarters Services, Directorate for Information Operations and Reports, 1215 Jefferson Davis Highway, Suite 1204, Arlington, VA 22202-4302, and to the Office of Management and Budget, Paperwork Reduction Project (0704-0188), Washington, DC 20503.

1. AGENCY USE ONLY (Leave blank)		2. REPORT DATE January 1992	3. REPORT TYPE AND DATES COVERED Final - May 1990 - August 1991
4. TITLE AND SUBTITLE Simulation in Infrared Imaging: Using Electrical Circuit Principles to Model Heat Transfer			5. FUNDING NUMBERS C - F33615-90-C-0005 PE - 63227F PR - 2743 TA - 25 WU - 17
6. AUTHOR(S) Ronald J. Evans			
7. PERFORMING ORGANIZATION NAME(S) AND ADDRESS(ES) University of Dayton Research Institute 300 College Park Avenue Dayton, OH 45469			8. PERFORMING ORGANIZATION REPORT NUMBER
9. SPONSORING/MONITORING AGENCY NAME(S) AND ADDRESS(ES) Armstrong Laboratory Human Resources Directorate Aircrew Training Research Division Williams Air Force Base, AZ 85240-6457			10. SPONSORING/MONITORING AGENCY REPORT NUMBER AL-TR-1991-0103
11. SUPPLEMENTARY NOTES Armstrong Laboratory Technical Monitor: Mr. Byron J. Pierce, (602) 988-6561			
12a. DISTRIBUTION/AVAILABILITY STATEMENT Approved for public release; distribution is unlimited.			12b. DISTRIBUTION CODE
13. ABSTRACT (Maximum 200 words) Simulation of thermal or infrared imaging involves modeling the heat exchange between database features and external sources of heat or radiation (e.g., the sun). One approach to computing differential scene irradiance, as viewed by a sensor, employs electrical circuit theory to model heat transfer between the database objects within the scene. In this report, practical shortcomings of this circuit approach and possible alternatives are introduced and analyzed. Heat storage (capacitance) was one process simulated. Results showed that the computational changes required to implement thermal capacitance are difficult to simulate numerically. Individual feature estimates of capacity were inconsistent with expectations. In addition, the temperature contribution from the capacity or time-varying component did not overcome the effect of the steady-state component, which contained a significant amount of error from assumptions made in the circuit model. Further work is required to identify approaches which provide less extreme object temperatures throughout a diurnal or daily cycle.			
14. SUBJECT TERMS Electrical circuit Forward looking infrared (FLIR) Irradiance Simulation Steady state temperature Thermal capacitance Thermal conductance			15. NUMBER OF PAGES 44 16. PRICE CODE
17. SECURITY CLASSIFICATION OF REPORT Unclassified	18. SECURITY CLASSIFICATION OF THIS PAGE Unclassified	19. SECURITY CLASSIFICATION OF ABSTRACT Unclassified	20. LIMITATION OF ABSTRACT UL

TABLE OF CONTENTS

	<u>Page</u>
SUMMARY.....	1
INTRODUCTION.....	1
REPRESENTING HEAT TRANSFER THROUGH ELECTRICAL CIRCUITS.....	2
THERMAL CAPACITANCE MODELING.....	11
CIRCUIT SOLUTION FOR TRANSIENT INPUT.....	25
CONCLUSIONS.....	31
REFERENCES.....	33

List of Figures

<u>Fig. No.</u>		
1	Surface Temperature as a Function of Time of Day (Arizona in August).....	3
2	Steady-State Feature Temperature Circuit.....	4
3	Idso-Jackson Estimate for Sky Irradiance as a Function of Air Temperature.....	8
4	Sun and Sky Irradiance Contribution to Feature Surface Temperature Model.....	9
5a	Circuit Representation with Capacitance for Massive Features.....	12
5b	Circuit Representation with Capacitance for Small Features.....	12
6	Steady-State Temperature Estimates for Capacitance Model.....	13
7	Feature Weights for Iterative Predictions (Short Time Scale).....	16

List of Figures (Concluded)

<u>Fig. No.</u>		<u>Page</u>
8	Feature Weights for Iterative Predictions (Long Time Scale).....	17
9	Iterative Capacitance Model Predictions for Weight = .34.....	23
10	Iterative Capacitance Model Predictions for Weight = .76.....	24
11	Sinusoidal Irradiance Estimates.....	26
12	Phasor Solution for Capacitance Model.....	29

List of Tables

<u>Table No.</u>		
1	Sample Feature Material Coefficients.....	18
2	Sample Feature Magnitude and Phase Coefficients.....	30

PREFACE

This project was conducted in support of the Armstrong Laboratory Human Resources Directorate, Aircrew Training Research Division, research concerning simulation of infrared imaging. This effort was managed by the University of Dayton Research Institute (UDRI), under Contract F33615-90-C-0005, Work Unit 2743-25-17 Flying Training Research Support. The laboratory contract monitor was Patricia A. Spears.

This effort supports the training technology objectives described in the present Armstrong Laboratory Research and Technology Plan. The goal of the present research was to provide an understanding of the computational aspects of the infrared imaging simulation and clarify the shortcomings in the computational model presently being used.

I wish to express my thanks to Ms. Marge Keslin for final edit of the manuscript.

Approved for	<input checked="checked" type="checkbox"/>
Dissemination	<input type="checkbox"/>
Classification	<input type="checkbox"/>
Other	<input type="checkbox"/>

SEL

v

A-1

SIMULATION IN INFRARED IMAGING: USING ELECTRICAL CIRCUIT PRINCIPLES TO MODEL HEAT TRANSFER

SUMMARY

One approach to computer simulation of infrared (IR) imaging is to model heat transfer between media using electrical circuit theory principles. A previous implementation of such an approach produced significant errors in surface temperature predictions for database features. The purpose of this effort was to reveal the source of these errors and explore alternatives.

Heat transfer is continuous across both space and time. For individual objects or features, heat transfer and storage are highly dependent upon individual material properties, exposure of features to the sun's radiation, and thermal insulation from objects beneath or adjacent to the feature of interest. Such characteristics make the building of general models quite susceptible to significant errors.

Analyses from this report revealed that: (a) some temperature prediction errors could be attributed to the discrete representation of database features and failure of the model to characterize thermal insulation for individual database features, and (b) inclusion of capacitance or heat storage capabilities in the model was problematic because material coefficients specific to individual features led to inconsistencies in the prediction of daily heating and cooling cycles for database features.

No simple solution to these problems exists. The desire to simulate the infrared signature of a large number of database features under a wide range of conditions necessarily requires a model of great complexity. The results of the present analyses provide a focus for future improvements in the model.

INTRODUCTION

Forward-looking infrared (FLIR) systems used on military aircraft are an integral part of the weapon systems package. Infrared imagery from the FLIR sensor is typically displayed on cathode-ray tubes (CRTs), appearing somewhat similar to black and

white television. To simulate the display of the FLIR image on the CRT, the scene irradiance from the database image impinging on the FLIR sensor is estimated, and computational procedures are employed to translate estimated irradiance into computer digital-to-analog code (DAC) values for display on a CRT.

Previous analysis of the IR imaging simulation software (Evans & Crane, 1990) in use at the Armstrong Laboratory, Human Resources Directorate, Aircrew Training Research Division (AL/HRA), at Williams AFB, AZ, documented inadequacies in the software predictions. Specific examples of shortcomings were the variability in diurnal feature surface temperatures and the inability of database objects to store or dissipate heat (i.e., thermal capacitance of objects) over time.

Figure 1 is a sample graph taken from Evans and Crane (1990). This graph denotes surface temperatures for 5 sample database features as a function of time of day. Interestingly, this graph is the wide fluctuation in the surface temperature of soil as the day progresses. For example, soil is much cooler than the other features during the early morning hours but heats up much more relative to the other features during the day. The FLIR impression, then, of the soil against a metal-based object during midday would be that the soil is hotter than the metal object. Given a scenario where pilots are using FLIR to locate or detect a metal structure during the day, their objective would be to find a hot area (i.e., the metal) in the midst of a cooler background (i.e., the soil). Therefore, such erroneous predictions by the software are of considerable concern.

REPRESENTING HEAT TRANSFER THROUGH ELECTRICAL CIRCUITS

The distribution of thermal energy in a system may be represented through analogy to an electrical circuit. Sources (e.g., the sun or sky) of radiant energy or flux measured in watts/m² may be represented as current within an electrical circuit. Conductance (or alternatively conductance⁻¹ = resistance) of heat across media, measured in watts/m²/°C (or °C/watt/m² for resistance), may be represented as conductance (resistance) in an electrical circuit, and temperature differences in a thermal system may be represented as voltage differences across elements of a circuit (Suits, 1985).

Figure 2 denotes one circuit representation of the steady-state temperature for a database object in thermal equilibrium. Input flux or current sources consist of the sun (P_{sun}) and the sky (P_{sky}). Radiation emanating from the database object of interest, P_{object} , is estimated through the Stefan-Boltzmann equation:

$$P_{\text{object}} = \epsilon \sigma T^4 \quad (1)$$

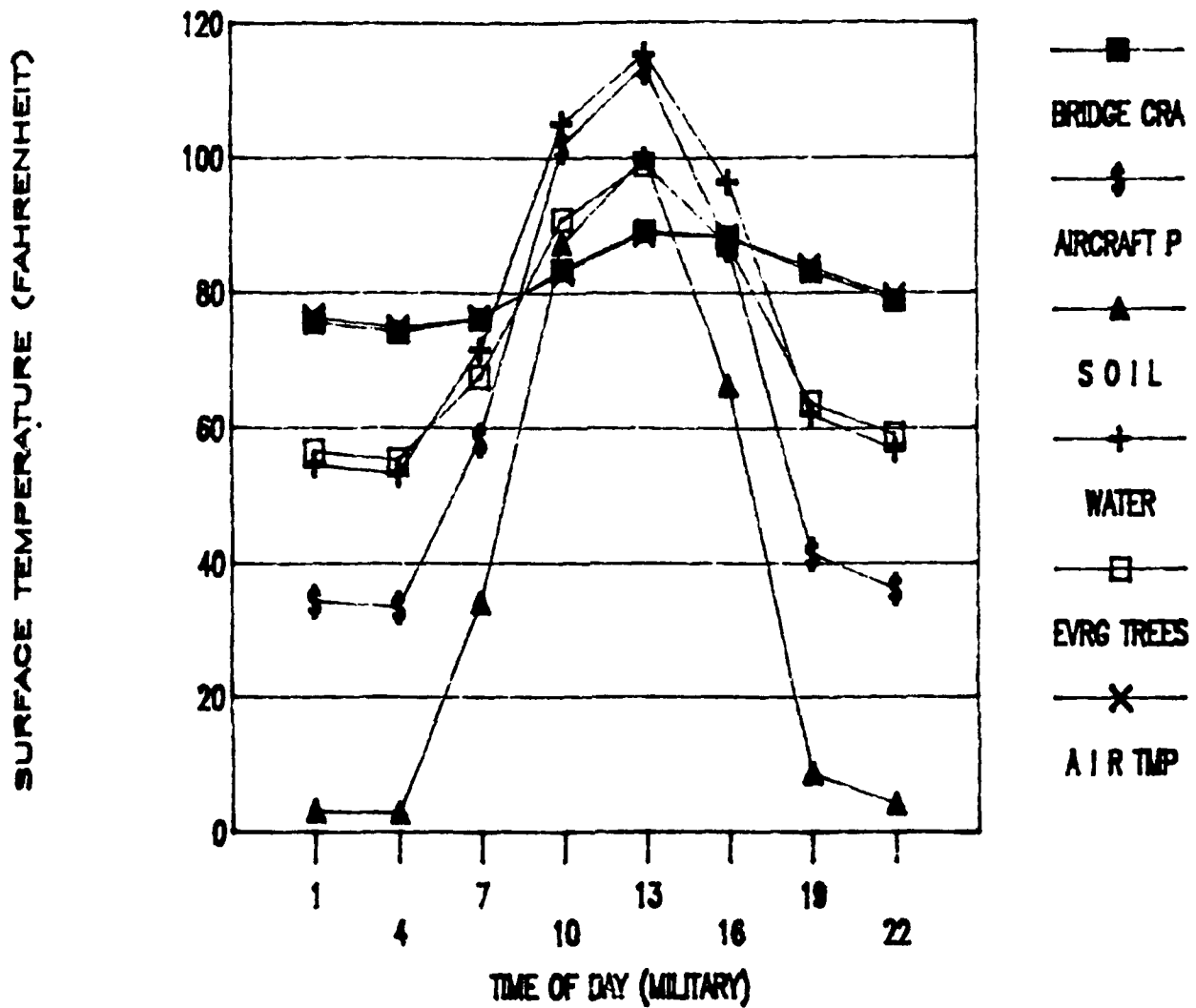


Figure 1. Surface Temperature as a Function of Time of Day (Arizona in August).

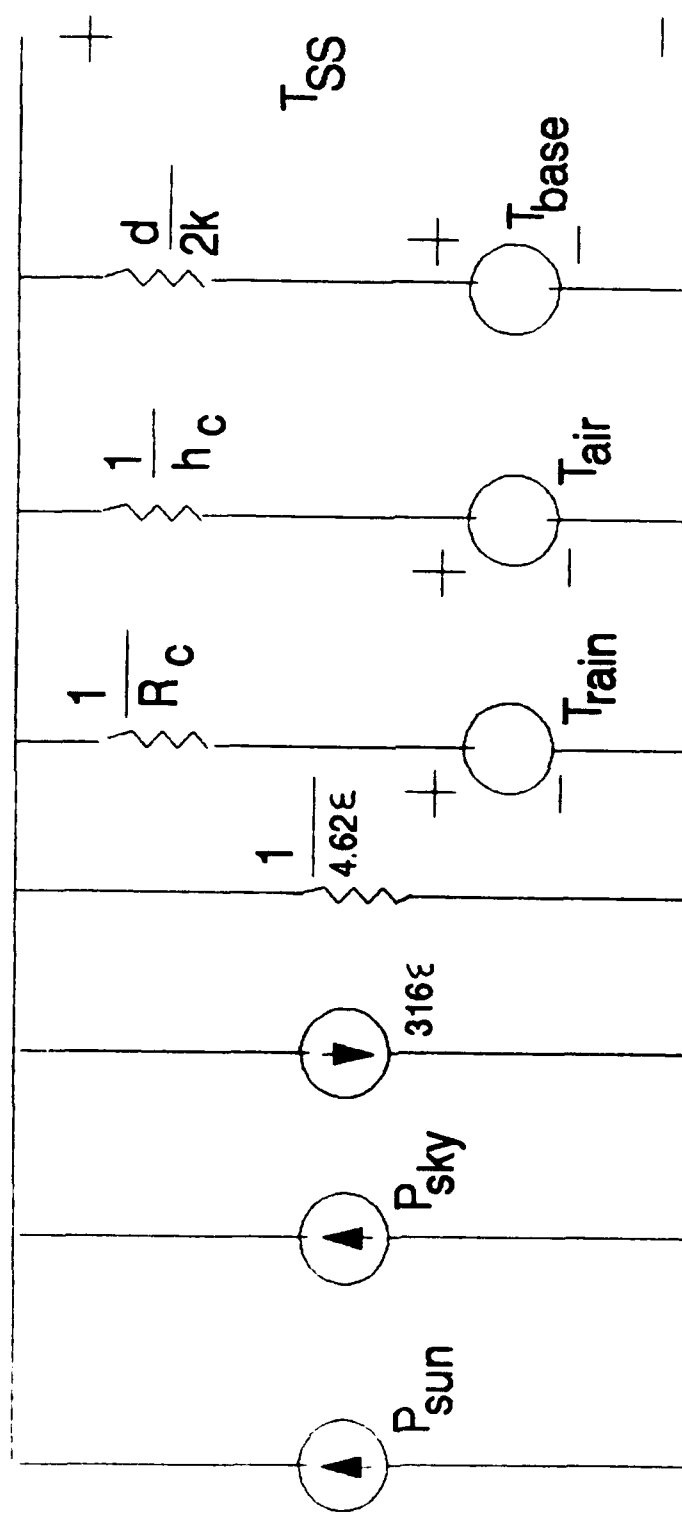


Figure 2. Steady-State Feature Temperature Circuit.

where ϵ is average material emissivity, $\sigma = 5.6686 \times 10^{-8} \text{ W/(m}^2 \text{ K}^4)$, and T is temperature in $^{\circ}\text{Kelvin}$. This 4th order equation of temperature is approximated in a linear fashion for circuit representation such that:

$$P = \epsilon \sigma T^4 = \epsilon (316 + 4.62T) \quad (2)$$

where T in the linear approximation is now in degrees Celsius. The circuit in Figure 2 shows 2 branches representing the 2 flux components, 316ϵ and $4.62\epsilon T$ (or $4.62\epsilon V$ where voltage is substituted for temperature), for the emission from the database object itself. Other branches of the circuit in Figure 2 represent independent temperature sources (rain, air, support base). Each source is modified by a conductance (resistance) across the other branches (i.e., h_k , h_c , and R_c ; the conductance across the feature of interest, from the wind, and from rainfall). Finally, in the steady-state or time invariant approach, the temperature (voltage) across the database object of interest is equivalent to the resistance of the database object multiplied by the flux through the database object and added to the temperature (voltage) of the base support (T_{base}).

Fourier's Law describes the rate of heat flux, P , through an object by the formula:

$$P = (k/d) (T_1 - T_2) \text{ in watts/M}^2 \quad (3)$$

where k is the thermal conductivity of the material in watts/(M $^{\circ}\text{K}$), d is the one-dimensional depth or thickness of the material, and T_1 and T_2 denote the temperature in $^{\circ}\text{K}$ on either side of the material. P is the flux which is analogous to current in our electrical circuit, the temperature difference ($T_1 - T_2$) in Fourier's Law is analogous to the voltage difference across a medium in an electrical circuit, and (k/d) represents conductance in either situation. Note that Figure 2 contains the resistance $d/(2k)$ and not d/k as shown in Fourier's Law. This change represents the amount of resistance across one-half the depth of the material and enables us to remain consistent with further developments of the model in this report when T_{base} will be replaced with a capacitor. The conductance parameters provide the rate of exchange per unit of temperature difference across objects contained in our closed system (e.g., database object, air, base support, rain).

The circuit in Figure 2 is a thermal model of the world from the perspective of the database feature of interest. Actual temperature gradients are continuous and all materials have some ability to capture and distribute thermal energy. Figure 2, then, is necessarily a simplification of the world from the database object's point of view. Along with this simplification, certain quirks of the representation can play an important role in determining surface temperature predictions. For example, when

there is no temperature (voltage) or radiant flux (current) input from any of the sources, the temperature or voltage difference across the branches is zero. Zero voltage denotes a surface temperature of 0 °C. Therefore, in the current implementation of the model, surface temperatures migrate toward freezing when the current and voltage sources contained in the model are set to zero. Feature surface temperature migration toward freezing is an important artifact of the model and shall be discussed in more detail later in the report.

The solution for feature surface temperatures in the original software is accomplished by using nodal and mesh analysis from circuit theory to solve for T_{ss} or voltage in Figure 2. The solution of T_{ss} in Figure 2 is:

$$T_{ss} = \frac{P_{sun} + P_{sky} - 316\epsilon + h_c T_{air} + h_k T_{base} + R_c T_{rain}}{4.6\epsilon + h_c + h_k + R_c} \text{ } ^\circ\text{Celsius (4)}$$

h_c , h_k , and R_c represent conductances for wind, the database object of interest, and rain, respectively. T_{air} , T_{base} , and T_{rain} represent temperature sources for air, a base of support, and the rain, all measured in °Celsius. Further explanation of Equation (4) can be found in Evans and Crane (1990) while the general approach can be found in Suits (1985). Equation (4) denotes a steady-state solution for feature surface temperatures, and Figure 1 denotes a plot of Equation (4) for the sample features. The steady-state solution applies when database features do not store or build up heat capacity for release at a later time. The calculation of surface temperature above serves for both small and massive objects in the current version of the software used at AL/HRA.

Before proceeding with modifications of Figure 2, it proves useful to examine a common scenario for the circuit in Figure 2 which will highlight problems inherent in the model. For a calm day with no wind or rain, h_c and R_c , the air conductance and the rain conductance, will be zero. Zero conductance amounts to infinite resistance, allowing no current to flow through the respective branches in Figure 2. The current or flux generated by the three independent generators, $P_{sun} + P_{sky} - 316\epsilon$ is then divided across 2 branches, the first with resistance $1/(4.62\epsilon)$ and the second with resistance $d/(2k)$ and independent temperature (voltage) source T_{base} which is generating current itself. The solution for T_{ss} is then:

$$T_{ss} = \frac{P_{sun} + P_{sky} - 316\epsilon + h_k T_{base}}{4.62\epsilon + h_k} \text{ } ^\circ\text{Celsius (5)}$$

P_{sun} and P_{sky} represent radiant flux from the sun and sky modified by the absorption coefficient of the specific database feature.

Radiant flux from the sky is estimated using the Idso-Jackson Equation (Suits, 1985):

$$P_{sky} = \sigma T_{air}^4 [1 - .261 \exp\{-7.77 \times 10^{-4} \times (273 - T_{air})^2\}] \quad (6)$$

where T_{air} is air temperature in °Kelvin and $\sigma = 5.6686 \times 10^{-8} \text{ w/(m}^2 \text{ K}^4\text{)}$ is the Stefan-Boltzmann Constant. Figure 3 shows a plot of P_{sky} as a function of air temperature in °F. A typical value for P_{sky} , not attenuated by material absorption, is 300 watts/m² (60 °F).

The absorption coefficients for each material vary as a function of wavelength, making it difficult to represent absorption for each material with a single scalar. However, for the sample features, soil typically had the lowest absorption with an average of .4 and water's absorption coefficient was typically about .99. Figure 4 shows irradiance absorbed from the sun and sky under specific conditions (Arizona in August, no wind or rain) for each of the sample features. While the contribution of the sky was estimated using the Idso-Jackson Equation, the contribution from the sun was estimated using tables from Suits (1985).

In Figure 4, irradiance absorbed by the sample features varies from approximately 85 to 145 watts/m² at night to a maximum between 590 and 980 during midday. $P_{sun} + P_{sky} - 316\epsilon$ (ϵ being between .9 and 1 for all features) could be as low as -215 for soil at nighttime or as high as 680 for water during midday. From this range of values in Equation (5), we add the product $h_k T_{base}$. The conductance, h_k , across an object to a base support with temperature, T_{base} , ranges from a minimum of 2.7 for soil to a maximum of 1052.6 for the bridge crane in the sample features. For soil, then, the numerator in Equation (5) is approximately $-215 + 2.7T_{base}$ at night where T_{base} is given in degrees Celsius. For T_{base} less than 80 °C (176 °F), then, the soil temperature will be less than 0 °C or freezing temperature.

Figure 1 shows the result of this effect where soil surface temperature dips quite low at night. In addition, because $h_k = 2.7$ for soil, which is quite low for our sample features, increases in P_{sun} during the day in Equation (5) will have a more dramatic effect on the change in soil surface temperature than the change in the surface temperature of other features. This effect is also emphasized in Figure 1.

Given these facts, we find that T_{ss} will be heavily dependent on h_k , the conductance (measured in watts M⁻¹ °C) across a feature ($h_k = 2k/d$ being halfway across a feature and k/d across the entire feature) which denotes the passage of flux to a base of support to which the feature is attached. As h_k increases, T_{ss} approaches T_{base} . For the 5 sample features in Figure 1 (bridge crane, aircraft parking, soil, water, and evergreen tree), h_k was 1052.6, 7.9, 2.7,

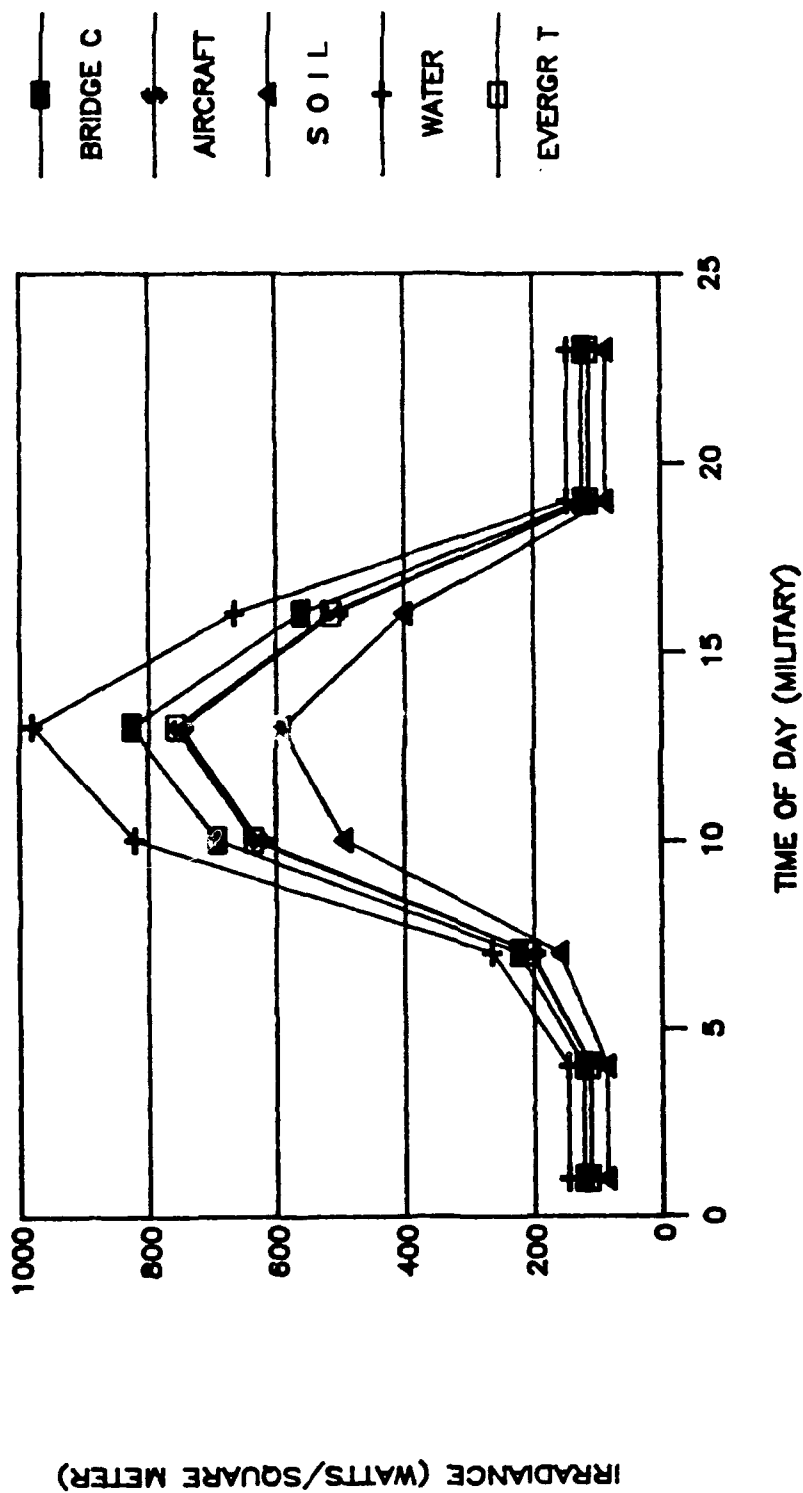


Figure 3. Idso-Jackson Estimate for Sky Irradiance as a Function of Air Temperature.

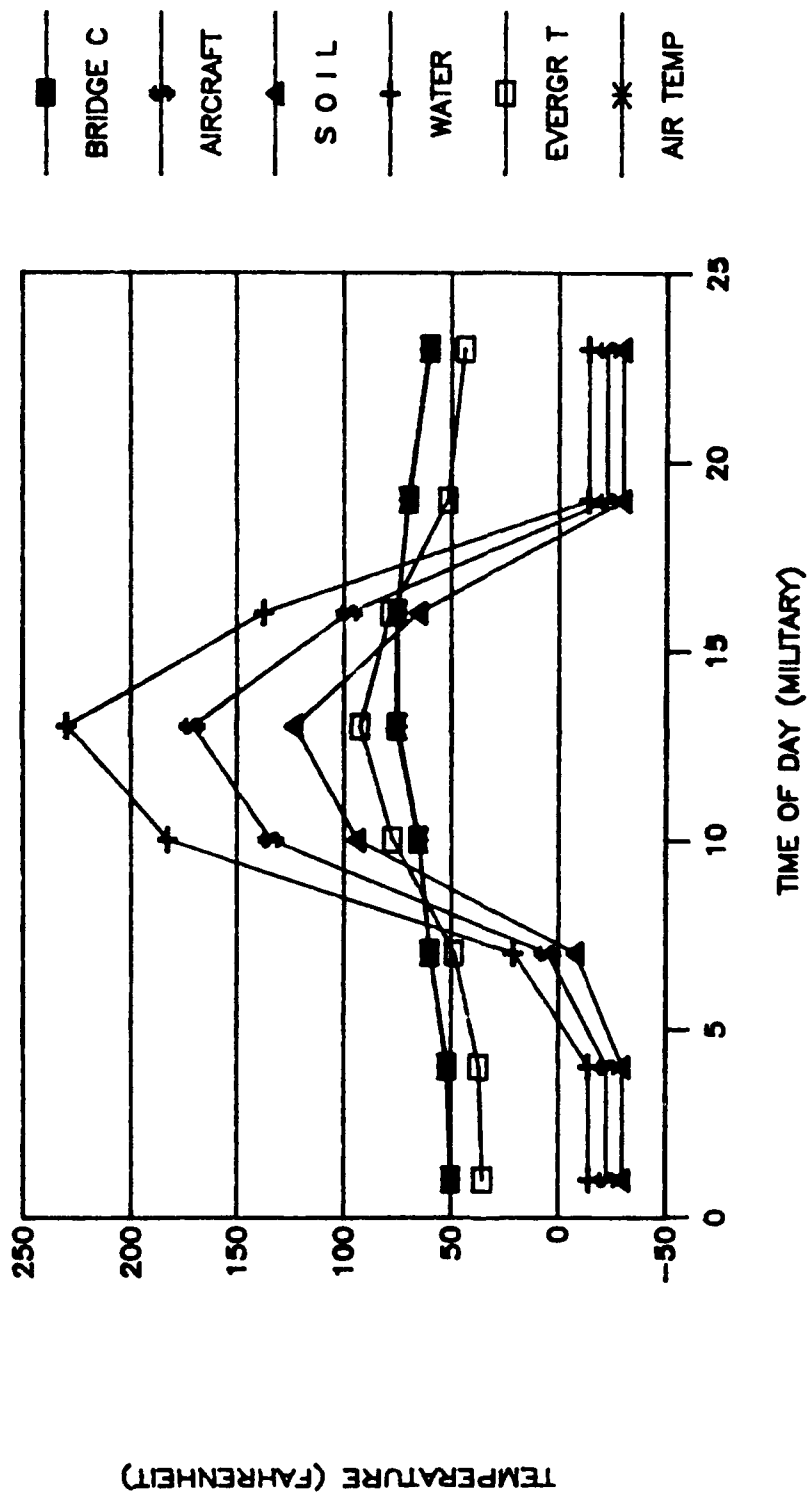


Figure 4. Sun and Sky Irradiance Contribution to Feature Surface Temperature Model.

19.1, and 25 ($\text{W M}^{-1} \text{ } ^\circ\text{C}$), respectively. For the bridge crane where $h_k=1052.6$, T_{ss} will always be approximately T_{base} . This version can be seen by inserting sample values into Equation (5). In the original version of the software, T_{base} was set to the air temperature and Evans and Crane (1990) found that the surface temperature of the bridge crane always mimicked the current air temperature quite closely.

The example above points out a shortcoming in the model from Figure 2. Metal in direct sunlight is able to attain temperatures much greater than the surrounding air temperature. In the model, however, the surface temperature of materials which are highly conductive (e.g., metals, aluminum) will approach T_{base} when the circuit from Figure 2 or Equation (4) is employed. Valid thermal modeling of these materials requires that they be allowed to store energy in some fashion.

Alternatively, soil is a very bad conductor with a conductance of $h_k = 2.7$. Figure 1 shows large variability throughout the diurnal temperature cycle of soil as mentioned in the last paragraph. For soil as represented in the circuit of Figure 2, then, with very little conductance to a base support, there is very little external input to maintain a reasonable temperature (i.e., anything above freezing or zero voltage) when flux input from the sun is near zero. In this specific instance, we realize that ground voltage for soil (or thermal support from beneath the surface) should probably be set near 60°F . A simple solution for soil would be to set the ground voltage to $+60$ (15.6°C) which would yield a circuit solution of:

$$T_{ss} = \frac{P_{sun} + P_{sky} - 316\epsilon + h_k T_{base}}{4.6\epsilon + h_k} + 15.6^\circ\text{Celsius} \quad (7)$$

which simply adds 15.6°C (60°F) to the steady-state temperature. This solution will not suffice, though, as a general solution because (a) it is not desirable to add 60°F to all feature surface temperatures, and (b) the same diurnal variation in soil surface temperature would exist which, as shown in Figure 1, is quite high.

Alternative solutions to this problem involve either (a) the addition of other temperature (voltage) sources which conduct heat to and from our feature of interest or, (b) allow our feature of interest to store and release heat over time. Alternative (b) has been studied more closely to date, so we will begin further analysis from this point of view and include modifications of alternative (a) along the way.

THERMAL CAPACITANCE MODELING

To allow database objects to store and release thermal energy over time, the circuit analogy must include a capacitor. A simple circuit representing database objects with heat storage and releasing capabilities was suggested by Hirsch (Personal Communication) similar to Suits (1985). Figure 5a is a duplicate of Figure 2 with the exception that the temperature source T_{base} has been changed into a capacitor which represents the temperature storage capability of the database object itself. Figure 5a is a circuit representation for massive database features. It does not include a base of support.

Using the principles of linearity and superposition, the solution for feature surface temperature, T , in Figure 5a can be broken into two components, a steady-state or forced component and a time-varying or natural component. By replacing the capacitor in Figure 5a with an open circuit, the steady-state temperature may be determined. Using circuit theory principles, steady-state surface temperatures for massive bodies (bodies which are at least a few feet thick) can be expressed as:

$$T_{ss} = \frac{P_{sun} + P_{sky} - 316\epsilon + h_c T_{air} + R_c T_{rain}}{4.6\epsilon + h_c + R_c} \quad ^\circ\text{Celsius} \quad (8)$$

The term "steady-state" used here is somewhat of a misnomer. The flux input from the sun and sky vary in a sinusoidal fashion throughout the day and, therefore, T_{ss} will not remain constant. T_{ss} is the result of applying the forcing function (i.e., the flux input) to the circuit in Figure 5a when no current flows down the path of the capacitor.

Since no flux flows down the path of the capacitor, T_{ss} in Equation (8) does not depend on h_k , the conduction across the feature of interest, as compared with Equation (4). Without the added resistance of $1/h_k$, Equation (8) is less stable than Equation (4).

Estimated surface temperatures for small database features are obtained from analyzing the network in Figure 5b. For small features, the steady-state surface temperature is the same as that in Equation (4) with the exception that $h_k = d/k$ instead of $d/(2k)$. The difference in the 2 representations is that in Equation (4) small objects are considered to be attached to a base support with temperature T_{base} . In Figure 5b, the capacitance network for small features, an extra path is included (from Fig. 5a) for a base of support. The conductance between the object and its support is $h_k = d/k$.

Figure 6 shows a plot of Equation (8) for both large and small features across a daily cycle with zero wind speed and rain (i.e.,

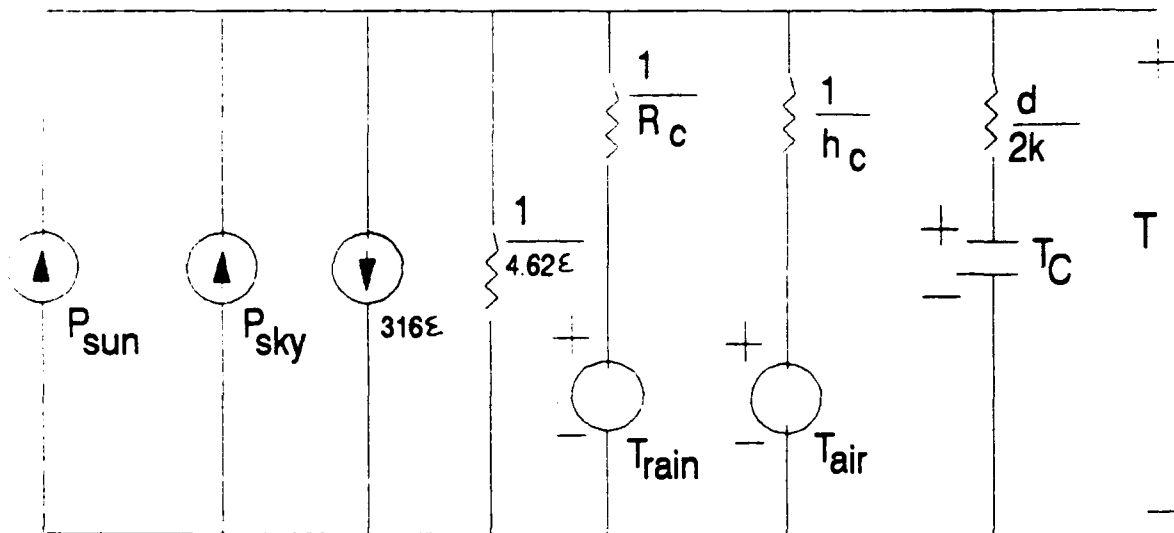


Figure 5a. Circuit Representation with Capacitance for Massive Features.

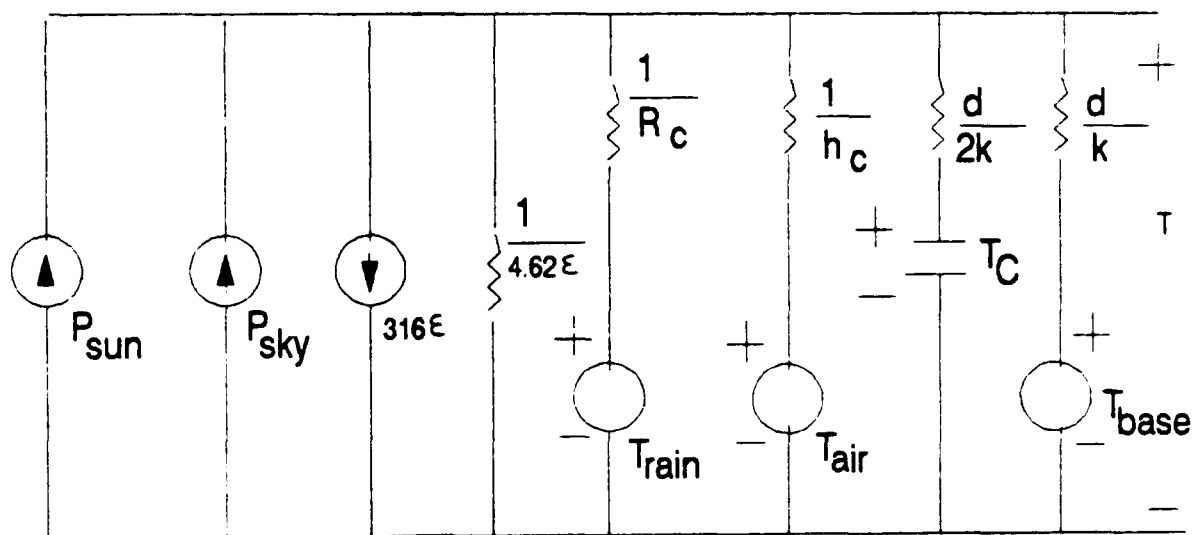


Figure 5b. Circuit Representation with Capacitance for Small Features.

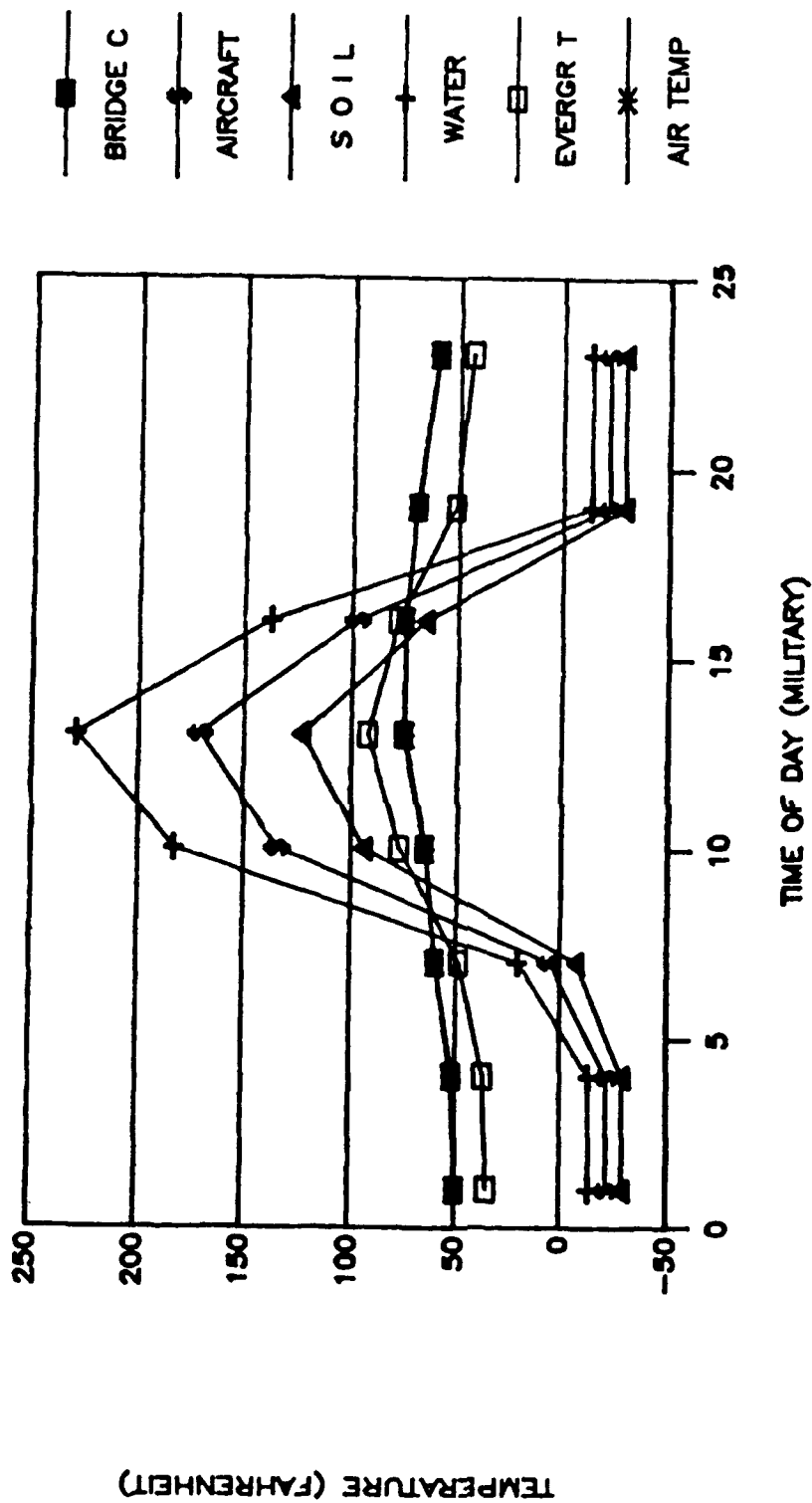


Figure 6. Steady-State Temperature Estimates for Capacitance Model.

both h_c and $R_c = 0$). Note the large variability in feature surface temperature across time for large features (asphalt, water, and soil). This variability is because these features are no longer attached to a base support as in Figure 2. Surface temperatures for small features (i.e., the bridge crane and the evergreen tree) in Figure 6 are not as variable across a diurnal cycle and, in fact, the surface temperature of the bridge crane directly mimics that of air temperature as previously found (see Fig. 1).

As can be seen by comparing Figure 6 with Figure 1, use of the capacitance model shown in Figure 5a will yield predicted feature surface temperatures for large features with a much wider range than the original circuit in Figure 2.

The complete surface temperature solution for constant radiant input proposed by Hirsch for massive bodies consisted of a combination of a steady-state or forced component and a time-varying or natural component:

$$T = T_{ss} - (T_{ss} - T_{oc}) e^{-\frac{t}{RC}} \left(1 - \frac{d/2k}{R}\right) \text{ } ^\circ\text{Celsius} \quad (9)$$

The passage of time in seconds is denoted as t . T_{ss} represents the steady-state temperature component described previously when the capacitor is replaced by an open circuit. T_{oc} represents the temperature of the database feature at time $t = 0$ or the initial condition of the feature. The resistance, R , denotes the resistance halfway across the feature itself, $R_1 = (d/2k)$, in serial with the remainder of the resistance throughout the circuit, $R_2 = (1/(h_c + R_c + 4.62\epsilon))$ for large features or $R_2 = (1/(h_c + R_c + d/k + 4.62\epsilon))$ for small objects so that $R = R_1 + R_2$. The term $d/(2k)/R$ denotes the relative weight of resistance flowing down the path of the capacitor to the entire resistance in the circuit. As this weight approaches 1 (i.e., there is infinitely more resistance down the path of the capacitor than the other paths), no current will flow down the path of the capacitor, the term $(1 - d/(2k)/R)$ approaches zero, and the time-varying component in Equation (9) approaches zero. Capacitance or C in Equation (9) is the product of the density and specific heat of the material composing the feature and one-half the depth of the feature. Therefore, thermal capacitance is a linear function of the thickness of the feature.

Components of Equation (9) can be recombined in order to view feature surface temperature, T , as a linear combination of the steady-state temperature, T_{ss} , and the initial temperature, T_{oc} . This restructuring is as follows:

$$T = T_{ss} - (T_{ss} - T_{oc})w(t) = (1 - w(t))T_{ss} + w(t)T_{oc} \quad (10)$$

where

$$w(t) = e^{-(t/(RC))} (1 - d/(2k)/R)$$

and $w(t)$ represents a time-varying weight plotted in Figures 7 and 8. $W(t)$ decays to zero for all features as time increases. This increase forces feature surface temperature (T) to migrate toward T_{ss} as time moves forward from the initial condition.

Individual feature material properties contributing to $w(t)$ are feature emissivity, thermal conductivity, material density, heat, and material depth or thickness. For the sample features, the first 4 coefficients are provided in Table 1. These coefficients are considered constants; however, they can vary somewhat as a function of temperature, humidity, etc. The final coefficient, d or feature thickness, has been mentioned previously as a source of concern within the model, affecting resistance and capacitance in the model. Feature thickness must be estimated (typically by the database modelers) in the database for small features and through computational estimation procedures for massive features (Suits, 1985). For massive features, feature thickness in meters is estimated as:

$$d = \left[\frac{86400k}{\pi ED} \right]^{\frac{1}{2}} \quad (11)$$

where k is thermal conductance, E is specific heat, and D is the material density for the database feature of interest. As mentioned previously, the assumptions accompanying Equation (11) may be somewhat suspect for the purpose of our application. The thickness, d , computed in Equation (11) for massive features, represents the maximum thickness of material involved in the diurnal heat transfer such that the temperature at this depth decays to $1/e$ or .368 of the surface temperature (see Suits, 1985). For the 5 sample features, estimates of d are provided in Table 1. The computed thickness of the massive features (aircraft parking, soil, and water) is greater than the thickness of the small features (bridge crane and evergreen tree). It is not clear, however, whether the relative differences in the thicknesses of the materials are appropriate.

Increments in the thickness, d , of a feature increases (a) the resistance of the feature to thermal flux, and (b) the capacitance of the feature. These increases, in turn, have an effect on both the steady-state temperature, T_{ss} , and the time-varying component, $(T_{ss} - T_{oc}) e^{-(t/(RC))} (1 - d/(2k)/R)$.

Increases in d cause a decrease in the conductance, h_k , from Equation (4), making the steady-state temperature of a feature more dependent on input from the sun, sky, rain, and air as opposed to any base support to which the feature is attached.

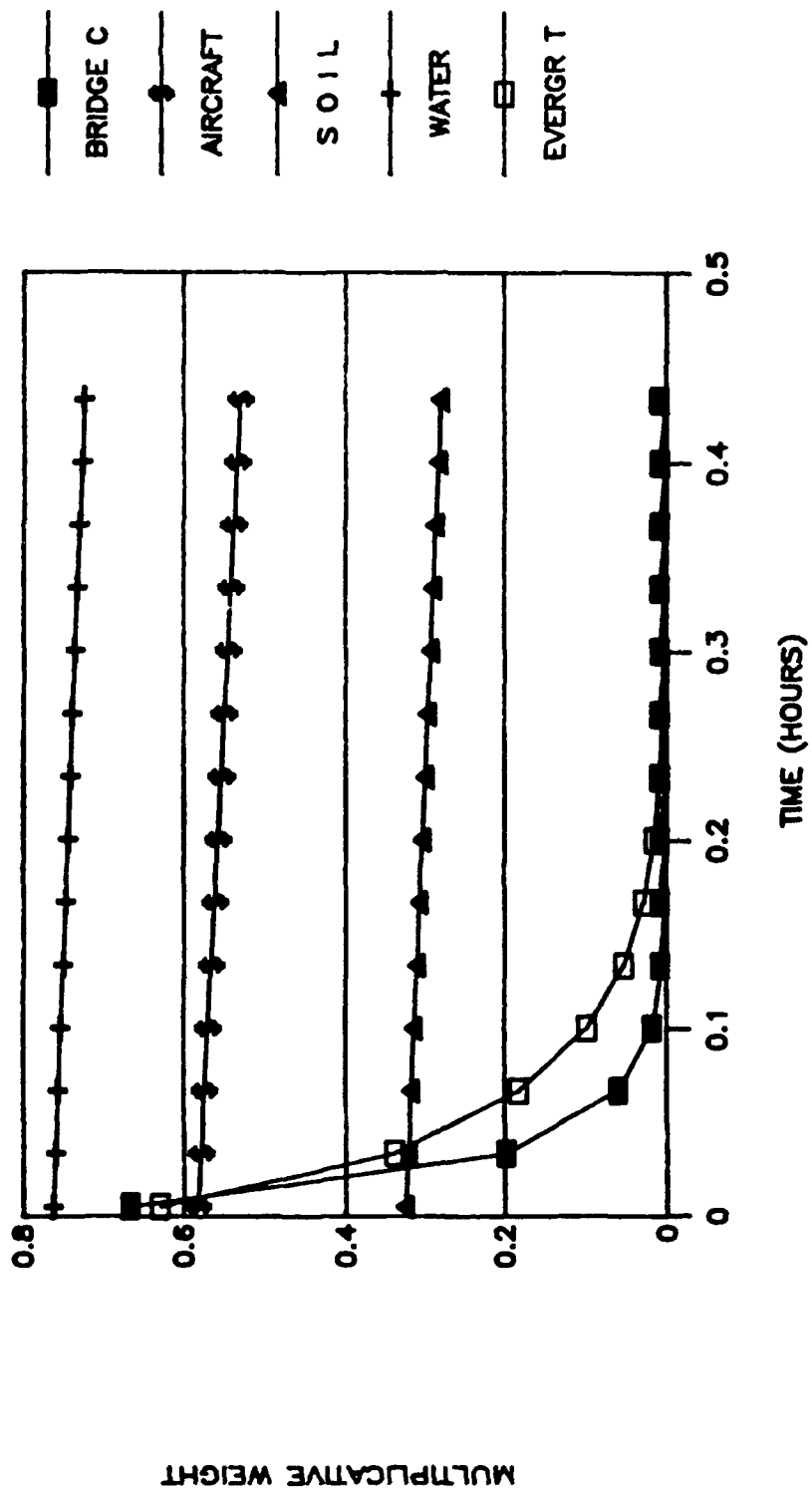


Figure 7. Feature Weights for Iterative Predictions (Short Time Scale).

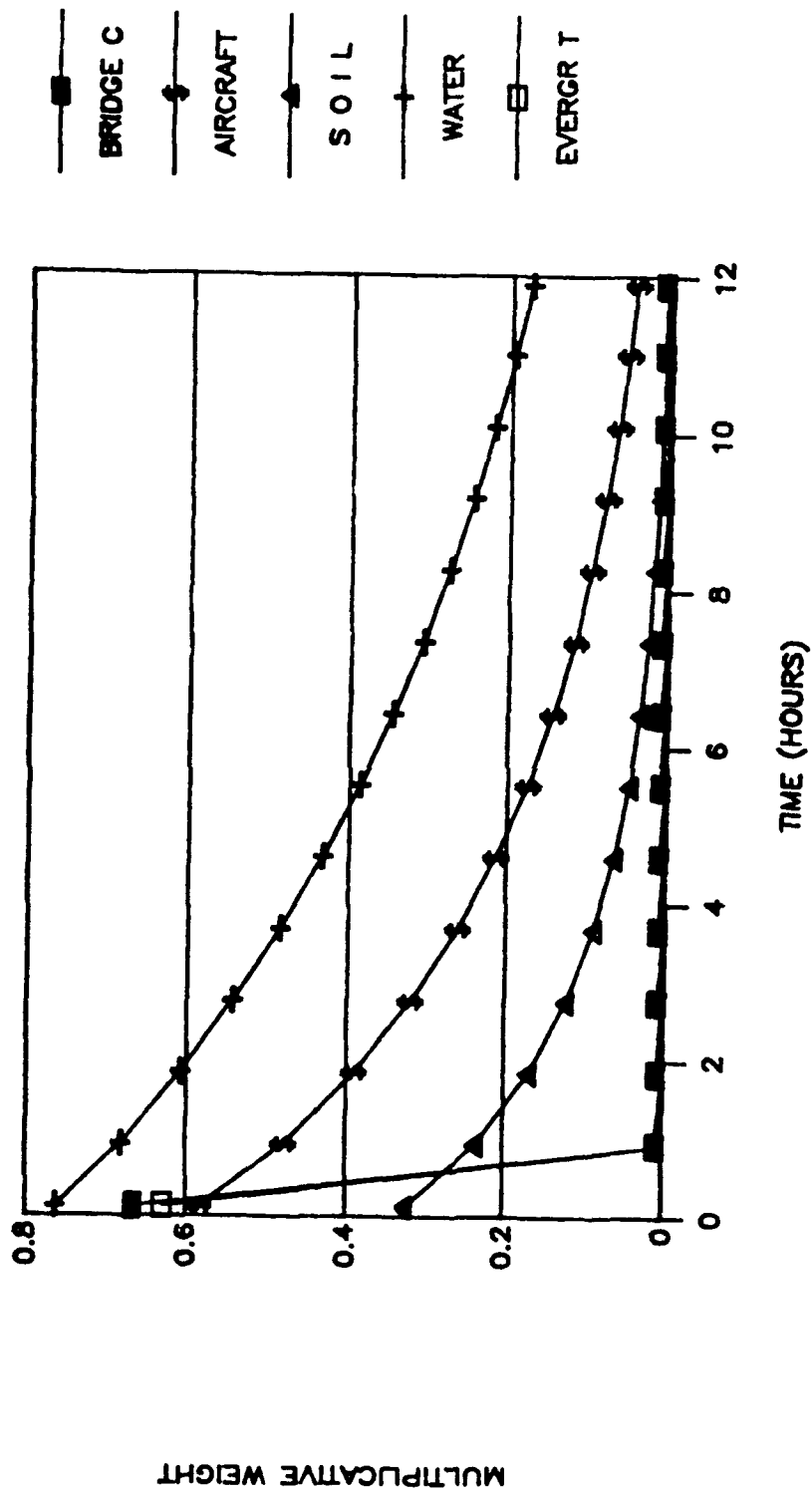


Figure 8. Feature Weights for Iterative Predictions
(Long Time Scale).

Table 1. Sample Feature Material Coefficients

	Bridge crane	Aircraft parking	Soil	Fresh water	Evergreen tree
Feature Type	small	massive	massive	massive	small
Estimated Thickness(meters)	.038	-	-	-	.006
Computed Thickness(meters)	-	.263	.092	.063	-
Density	7800	500	466	1000	500
Thermal Conductivity (k)	40	1.047	.1260	.6	.15
Specific Heat (E)	470	830	879	4180	2400
Capacitance (C)	69654	54572	18842	131670	3600
Feature Conductance 2k/d	2105	8	2.7	19	50
Capacitance Circuit Resistance (R)	.00142	.355	.6	.28	.054

Massive objects do not resist the input flux more because of their thickness or size as the model from Equation (9) would currently indicate. These objects distribute the thermal energy throughout the material. This notion, however, is indicative of greater capacitance and should be reflected through the capacitance parameter. Soil, for example, is a massive object which, although it does not conduct thermal energy well, has great capacity for distributing the thermal energy it does conduct. Six to twelve feet below the surface, the temperature of the earth remains constant at approximately 60 °F. The temperature gradient from the surface of the earth to a depth of 6 feet is continuous. This continuity constraint limits the effect of radiant energy or atmospheric air temperature in modifying the temperature at the soil's surface. In the thermal modeling of soil, this constraint could be modeled by placing a resistor of value d/k where $d = 2$ meters and k is .1260 and a voltage source of 60 °F or 15.6 °C below the capacitor representing soil in the circuit.

The thickness of the soil layer, however, should not affect soil's ability to receive radiant flux. Soil, however, also has low thermal conductance, k , as opposed to metal. Thermal conductance is inversely related to the resistance of a material to thermal flux as one may attest to by comparing the feel of metal with that of a piece of soil on a hot summer day. The use and placement of an object's resistance, d/k , in our circuit model is misleading. Placing this resistance in front of our capacitor prevents thermal flux from entering the capacitor. As can be inferred from Fourier's Law, this resistance should actually apply only to objects on the opposite side of the feature of interest. This resistance is one of the problems of representing thermal gradients, which are continuous in space, with discrete circuit models. This source of error plays a major role in the thermal model.

To estimate the initial temperature, T_{oc} , from Equation (9), Hirsch suggested that the software could be run at 20-min intervals 1 day prior to the estimate of T_{oc} actually desired. T_{oc} should be set to zero for the initial run (" i " = 1) with subsequent values of T_{oc} on computer run " $i + 1$ " set to the final estimate of T for the respective feature from run " i ."

In Equation (9), the final feature surface temperature, T , will be the steady-state temperature T_{ss} modified by a time-varying component which will be a percentage of the difference between T_{ss} and T_{oc} . The decaying exponential in the time-varying component, $e^{-t/(RC)}$ (where t is expressed in seconds), places less weight on the time-varying component, $(T_{ss} - T_{oc})$, as time passes. The other weight in the time-varying component, $(1 - d/2k/R)$, denotes relative resistance down the path of the feature of interest to the entire circuit and varies between zero and one. If the resistance $d/(2k)$ down the path of the capacitance is quite large relative to the total resistance of the circuit, very little flux will flow into the capacitor and there will be no charging of the capacitor, or equivalently, no thermal heating of the feature. In this instance, the term $(1 - d/(2k)/R)$ will be approximately zero and the feature surface temperature will always be the steady-state temperature T_{ss} .

The thermal heat transfer process is continuous in time and three-dimensional space. The electrical circuit is composed of discrete elements. For example, in the circuit model the resistance to flux input at the feature capacitor is $d/(2k)$. This simple representation means that the flux travels through half of the material, $d/2$, before it reaches the capacitor. As the depth of the material d increases, less flux reaches the capacitor. This is a discrete representation of a continuous process. In an actual feature of reasonable size, a temperature gradient will exist across the material of interest and capacitance exists throughout the material, not just at a depth of $d/2$. For example, large metal objects heated on one side may exhibit a large temperature gradient from the heated or sunny side to the underside. Soil, which is one

of the sample features of interest in this report, is a poor conductor of thermal energy and will not heat up like metal in response to the sun. Six feet below the surface, soil temperature remains stable at approximately 60 °F. To properly model surface temperature, this gradient from below the surface to the surface of the soil should be properly modeled. Although the example described here can be more accurately modeled through discrete circuitry than is presently the case, it would be necessary to implement such improvements on a feature-by-feature basis.

The characteristics of the time-varying weights, $e^{-(t/(RC))}$ and $(1 - d/(2k)/R)$, may be analytically studied to determine their general influence on feature surface temperature estimation, or for approximating T_{oc} , as Hirsch suggested. If either of the weights or the combination of weights approaches zero, the time-varying component of the surface temperature equation will not contribute to Equation (9). Figures 7 and 8 show the multiplicative combination of weights (i.e., $e^{-(t/(RC))} (1 - d/(2k)/R)$) for the time-varying components of feature surface temperatures for the 5 sample features (bridge crane, aircraft parking area, soil, water, and an evergreen tree). Note that the aircraft parking area, soil, and water are considered massive objects while the bridge crane and evergreen tree are small objects.

At time zero in Figures 7 or 8, the decaying exponential is simply $e^0 = 1$ and the multiplicative weight for each sample feature becomes $(1 - d/(2k)/R)$. According to the model, water provides the least amount of resistance to heat with a weight in the neighborhood of .76 at a time of zero. This finding is shown in Figures 7 and 8. As mentioned previously, the component $(1 - d/(2k)/R)$ represents the resistance the radiant flux meets from the feature of interest relative to the components in the circuit. Large features might show more capacitance but not necessarily more resistance to flux at the surface. For example, in Figure 5, water shows more resistance to incoming flux than does the evergreen tree. This is not logical as we would expect that water conducts thermal radiation more readily than an evergreen tree.

The decay of the curves in Figures 7 and 8 is determined by their time constants, $1/(RC)$, from the exponent in Equation (9). The larger the time constant, the more rapid is the decay of the curve in Figures 7 and 8. Smaller time constants (larger RC values) represent capacitors which take longer to store up energy as well as dissipate energy. Thus, we might expect that massive objects would have smaller time constants (larger RC values) because thermal energy should build up as well as dissipate more slowly over time for these objects. This premise holds true as expressed in Figures 7 and 8. In Figure 8, decay rates of the sample massive features are available. Soil has the fastest decay, followed by the aircraft parking area and water. These storage and dissipation rates do not meet our intuitive expectations. Logically, we would expect soil to have the slowest uptake and

release of heat, followed by water and then asphalt from the aircraft parking area. Mathematically, these expectations would be reflected in the RC combinations with:

$$RC_{\text{water}} < RC_{\text{aircraft p}} < RC_{\text{soil}} \quad (12)$$

or equivalently

$$1/RC_{\text{water}} > 1/RC_{\text{aircraft p}} > 1/RC_{\text{soil}}. \quad (13)$$

In the time constants $1/(RC)$ we can compare both the values of R and C for small versus large features. As expressed previously, $R = d/(2k) + 1/(4.6\epsilon + h_c + R_c)$ for large features and $R = d/(2k) + 1/(4.62\epsilon + h_c + R_c + k/d)$ for small features and only d and k , the material depth and conductivity, change significantly across features. When there is no rain or wind, $1/(4.6\epsilon + h_c + R_c)$ is approximately .23 and R becomes approximately $d/(2k) + .23$ for large features. For small features, R is approximately $[(3k + 4.37d)/(k + 4.37d)] \times d/(2k)$. Estimates of R under conditions of no rain or wind are given in Table 1 for the sample features. Capacitance or C in the term $1/(RC)$ is the product of material density, the specific heat of the material, and one-half the depth of the material. Capacitance for each of the sample features is given in Table 1. As can be seen from Table 1, soil has the smallest estimated capacitance. This finding is not as expected and, in fact, the ground or soil stores and releases thermal energy much more slowly than small bodies of water. The value of d , the thickness of the soil, could be increased to increase C , the capacity for soil, relative to the other sample features. Estimation of material thickness for massive features was accomplished through Equation (11), as previously mentioned, and these estimates are provided in Table 1. In the present model, capacitance is a linear function of the depth of the features so that doubling the depth of a feature would also double the capacitance. In Table 1 we see that the depth of the massive features (soil, aircraft parking area, and water) is not necessarily greater than the depth of the small features (bridge crane and evergreen tree).

Intuitively, then, the relative ordering of the thicknesses for the 5 features in Table 1 is questionable. Because massive feature depths are estimated from Equation (11), the use of Equation (11) in estimating material depth for use in capacitance is considered questionable.

Given this consideration of estimating feature thickness, we can return to the problem of approximating Equation (9) through numerical iteration. Hirsch suggested that feature temperature estimates, T , be computed every twenty minutes with T_{∞} initially set to zero. On each subsequent iteration, then, T_{∞} is set to the value of T computed on the previous iteration. From Figure 7 we can estimate that, at one-third of an hour, the time-varying weights for the small features, the bridge crane and the evergreen tree, are approximately zero. This results in the estimate of T

always being approximately T_{ss} . For the massive features of water, the aircraft parking area and soil, the weights at $t =$ one-third hour (from Fig. 8) are approximately .76, .58, and .34, respectively. New estimates of soil surface temperature, then, are 66% of the current feature steady-state temperature plus 34% of the surface temperature of the soil from 20 min prior.

We can ask how this reformulation, using the time-varying component, modifies feature surface temperatures across a diurnal cycle. Our general goal (looking back to Fig. 1) is to soften the extreme temperature variation for features such as soil. The iterative approach suggested by Hirsch (iteration every 20 minutes to update feature surface temperature) leads to the equation:

$$T_{i+N} = P^N T_i + (1 - P) \sum_{j=0}^{N-1} P^j T_{ss(i+j+1)} \quad (14)$$

where T_i is the feature surface temperature on iteration "i," T_{i+N} is the feature surface temperature on iteration "i + N," $T_{ss(i+j+1)}$ is the steady-state temperature on iteration "i + j + 1," and P denotes the weight, $w(t) = e^{-(t/(RC))} (1 - d/(2k)/R)$, from Equation (10). Equation (14) shows that the feature surface temperature at any time is a weighted combination of: (a) the feature surface temperature at any previous time plus, and (b) a sum of steady-state temperatures between the initial period and the present time. Figures 9 and 10 show estimates of Equation (11) for soil ($P = w(t) = .34$) and water ($P = w(t) = .76$), respectively. The steady-state temperature in Figures 9 and 10 is a sine wave used to approximate diurnal variation. In both Figures 9 and 10, the initial feature surface temperature at time zero or "i" = 0 is $X_i = 0$, as Hirsch suggested. Iterative updates in Equation (14) were made every 20 min. As can be seen from Figures 9 and 10, the iterative estimates quickly fall into line with the sine wave as time passes. As the value of P increases from .34 (soil) (Fig. 9) to .76 (water) (Fig. 10), the iterative estimate tends to lag more behind the steady-state input but the effect is still minimal.

As mentioned previously, our goal in adding heat storage capacity to the model was twofold. First, it was necessary to soften extreme surface temperature values across the daily heating and cooling cycle, as exemplified by soil in Figure 1. Second, it was desirable to create a time lag such that massive features heat slowly over the day and release heat slowly as the air temperature cools after the sun goes down. The surface temperatures predicted by the present iterative model will not perform either of these functions because the iterative estimate closes in on the steady-state temperature too quickly in time.

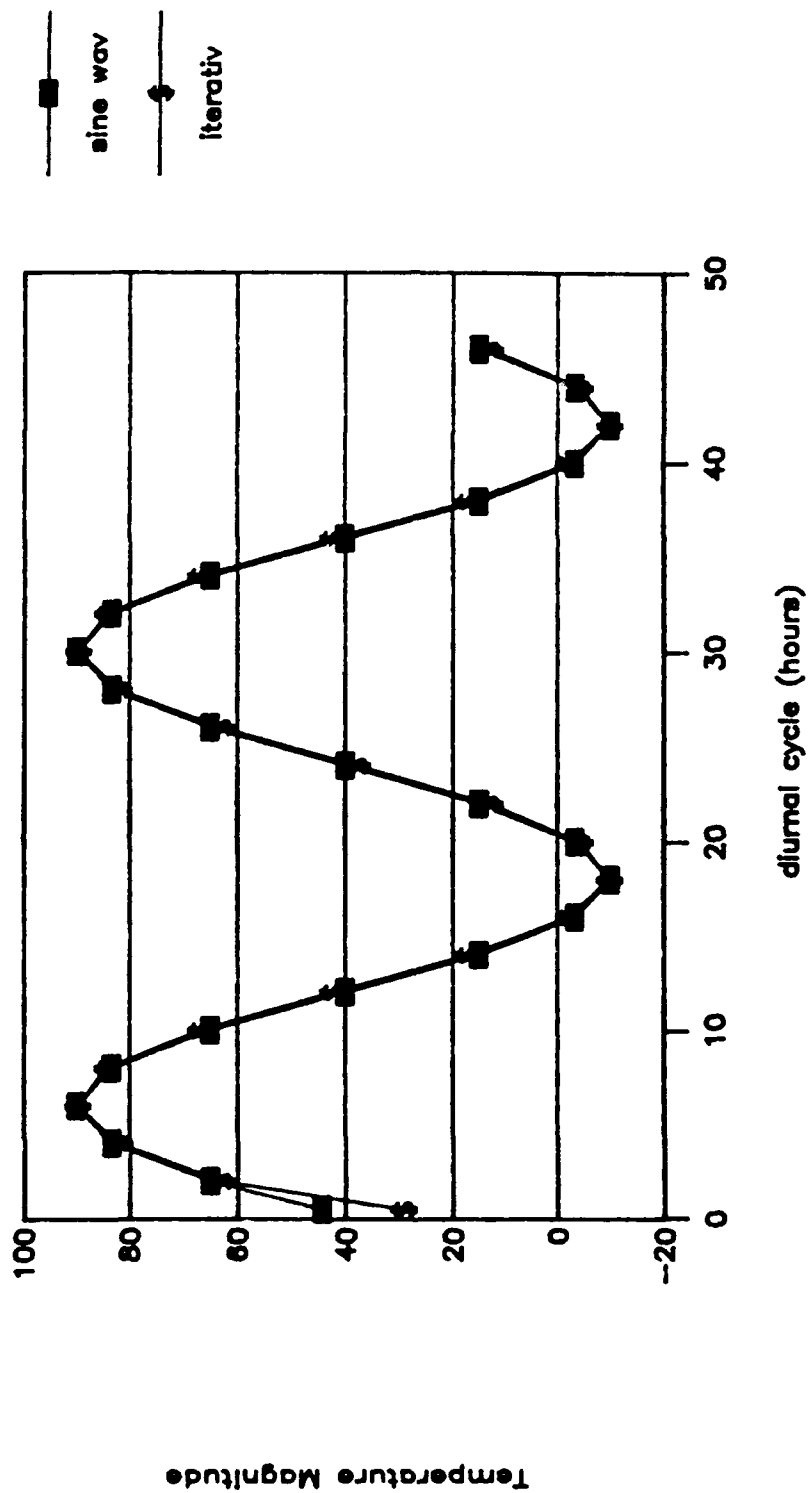


Figure 9. Iterative Capacitance Model Predictions for Weight = .34.

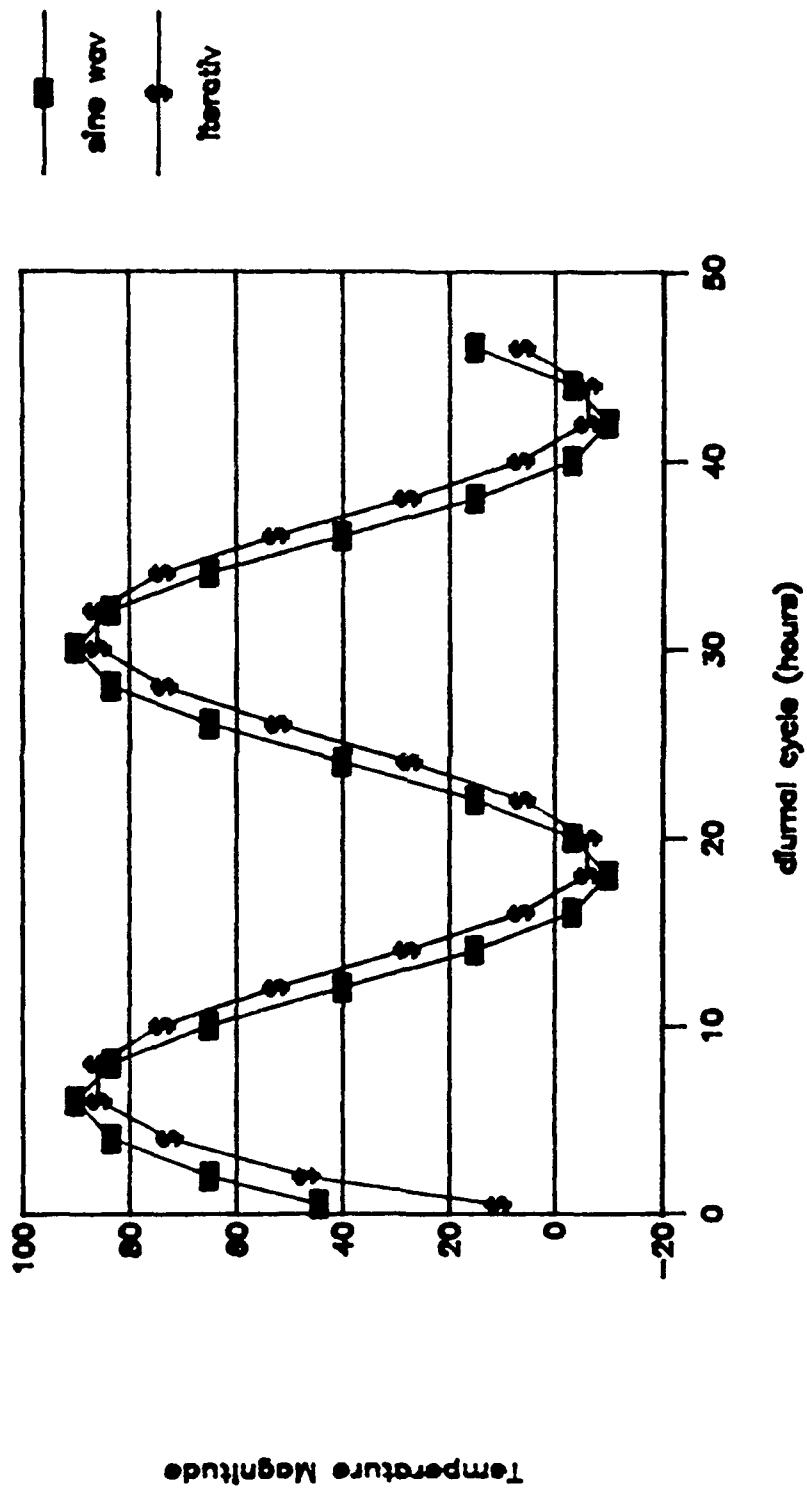


Figure 10. Iterative Capacitance Model Predictions.
for Weight = .76.

CIRCUIT SOLUTION FOR TRANSIENT INPUT

The surface temperature solution provided by Hirsch from Equation (9) in the previous section, $T = T_{ss} - (T_{ss} - T_{pc})e^{-(t/(RC))}(1 - d/(2k)/R)$, is a solution to a first-order differential equation with constant input flux. Flux input from the sun and sky does vary in a sinusoidal fashion across a diurnal cycle; however, the solution provided above is an approximation for slow changes in input flux relative to the response of the storage element(s). In this section, a more complete solution is provided to the network from Figure 2 in order to compare performance of the more complete solution with the approximation from the previous section.

Flux input from the sky and sun minus the constant (316 ϵ) from the linear black body approximation may be represented by a sinusoidal waveform of the form:

$$P_{sun} + P_{sky} - 316\epsilon = A \sin(\omega t - \theta) + B \quad (15)$$

where t is expressed in seconds and $t = 0$ designates midnight, $\omega = 2\pi f = 2\pi$ (1 cycle/day) = 2π (1 cycle/86,400 seconds) = 7.27×10^{-5} radians/second, $\theta = \pi/2$ designating 2 a.m. as the time of lowest flux input from the sun and sky, and $B - A$ being the minimum flux input (occurring at 2 a.m.) while $A + B$ denotes the maximum flux input (occurring at 2 p.m.) across the diurnal cycle. Figure 11 shows a sample plot of Equation (15).

Employing Equation (15) from above in the circuit in Figures 5a and 5b yields a nonhomogeneous first-order differential equation. Using circuit theory properties of linearity and superposition, the solution for T , the feature surface temperature, may be arrived at by solving the circuit for the response to the sinusoidal input ($A \sin(\omega t + \theta)$) and the constant input (B) separately, and then adding the two responses together. The feature surface temperature solution for the constant input is the solution to Equation (9), the homogeneous first-order differential equation provided in the last section of the form:

$$T_1 = T_{ss} - (T_{ss} - T_{oc})e^{-(t/(RC))}(1 - d/(2k)/R) \text{ } ^\circ\text{Celsius} \quad (16)$$

All of the parameters in Equation (16) are the same as in Equation (9) with the exception of the steady-state temperature which now takes the value:

$$T_{ss} = \frac{B + h_c T_{air} + R_c T_{rain}}{4.6\epsilon + h_c + R_c} \text{ } ^\circ\text{Celsius} \quad (17a)$$

for massive features, and

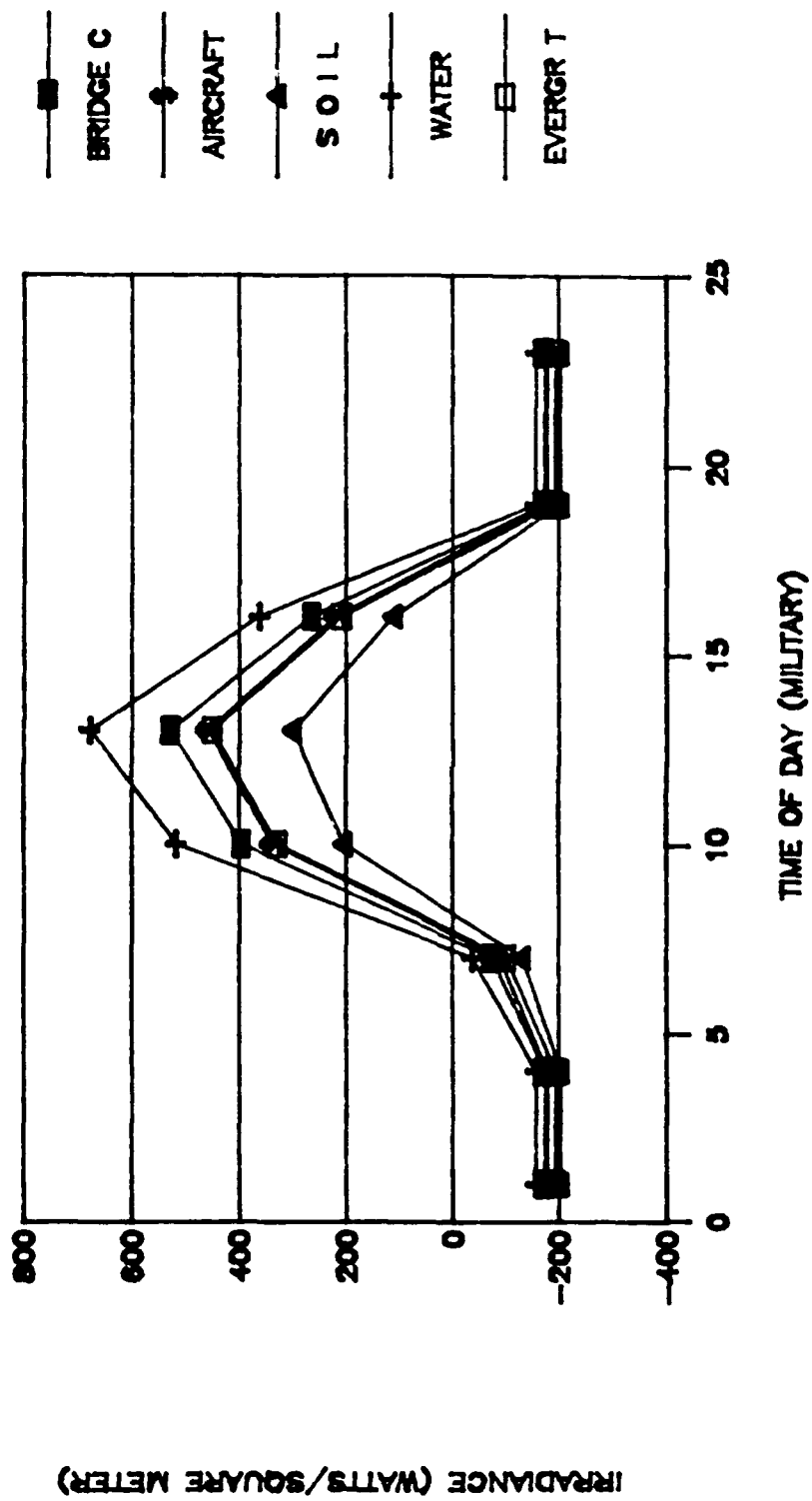


Figure 11. Sinusoidal Irradiance Estimates.

$$T_{ss} = \frac{B + h_c T_{air} + R_c T_{rain} + (k/d) T_{base}}{4.6\epsilon + h_c + R_c + (k/d)} \quad ^\circ\text{Celsius} \quad (17b)$$

for small features. All parameters in Equations (17a) and (17b) are identical to Equation (8) with the exception of B, the constant flux input from Equation (15).

The response to the sinusoidal input, $A \sin(\omega t + \theta)$, may be obtained using the Laplace Transform, yielding a feature surface temperature

$$T_2 = R \sin(\omega t + \theta + \theta_1) \quad (18)$$

where

$$R = \frac{A + h_c T_{air} + R_c T_{rain}}{\left[(4.62\epsilon + h_c + R_c)^2 + \frac{2(\omega C)^2}{(1 + (\omega C \frac{d}{2k})^2)^2} + 2(4.62\epsilon + h_c + R_c) \frac{\omega C}{1 + (\omega C \frac{d}{2k})^2} \right]^{\frac{1}{2}}}$$

and

$$\theta_1 = \tan^{-1} \left[\frac{\frac{-\omega C}{1 + (\omega C \frac{d}{2k})^2}}{4.62\epsilon + h_c + R_c + \frac{\omega C}{1 + (\omega C \frac{d}{2k})^2}} \right]$$

for massive features, and

$$R = \frac{A + h_c T_{air} + R_c T_{rain} + \frac{k}{d} T_{base}}{\left[(4.62\epsilon + h_c + R_c + \frac{k}{d})^2 + \frac{2(\omega C)^2}{(1 + (\omega C \frac{d}{2k})^2)^2} + 2(4.62\epsilon + h_c + R_c + \frac{k}{d}) \frac{\omega C}{1 + (\omega C \frac{d}{2k})^2} \right]^{\frac{1}{2}}}$$

with

$$\theta_1 = \tan^{-1} \left[\frac{\frac{-\omega C}{1 + (\omega C \frac{d}{2k})^2}}{4.62e + h_c + R_c + \frac{k}{d} + \frac{\omega C}{1 + (\omega C \frac{d}{2k})^2}} \right]$$

for small features. T_2 is a sinusoidal waveform which follows the sinusoidal form of the input flux from the sun and sky with the exception of a change in magnitude and a phase lag, denoted by R and θ_1 , respectively.

Figure 12 shows a plot of Equation (18) for the 5 sample features. Note that the temperatures in Figure 12 fluctuate around 0 °F. The DC (direct current) or average temperature component is not included in Equation (18) nor in Figure 12. Figure 12 shows only the variability in temperature across a diurnal cycle. Certainly the range in temperatures across a single day for individual features in Figure 12 is too large. For example, in Figure 12 evergreen trees have a range of approximately 120 °F and water has a range of approximately 60 °F. This shortcoming directly follows from the resistive inputs to the magnitude, R , in Equation (18) and can be attributed to inadequacies in the circuit model. The conclusion here is that another parallel conduit or path in the circuit model is required to carry more thermal flux away from the feature of interest.

The important parameters in Figure 12 are the magnitudes of the sine waves, R , which represent minimum and maximum daily heat values, and the phase shift, θ_1 , which represents time lag in the buildup and release of heat throughout a daily cycle. For the 5 sample features, these values are presented in Table 2.

Estimates of magnitudes in Table 2 are much like estimates of T_{ss} in the initial part of this report. If we include a base of support in the circuit model as we have done with small features, the magnitudes will be dependent upon the base support temperature to the extent that feature conductance, $h_k = k/(2d)$, outweighs all other conductances. For the bridge crane, h_k is quite large (see Table 1), forcing the magnitude, R , to be approximately the base temperature (air temperature). For the evergreen tree, h_k is much more in line with other conductance values in the circuit, and R tends to be an averaging of air temperature with irradiance from the sun and sky. For the massive features, the estimated temperature magnitudes are dependent upon the irradiance from the sun and sky.

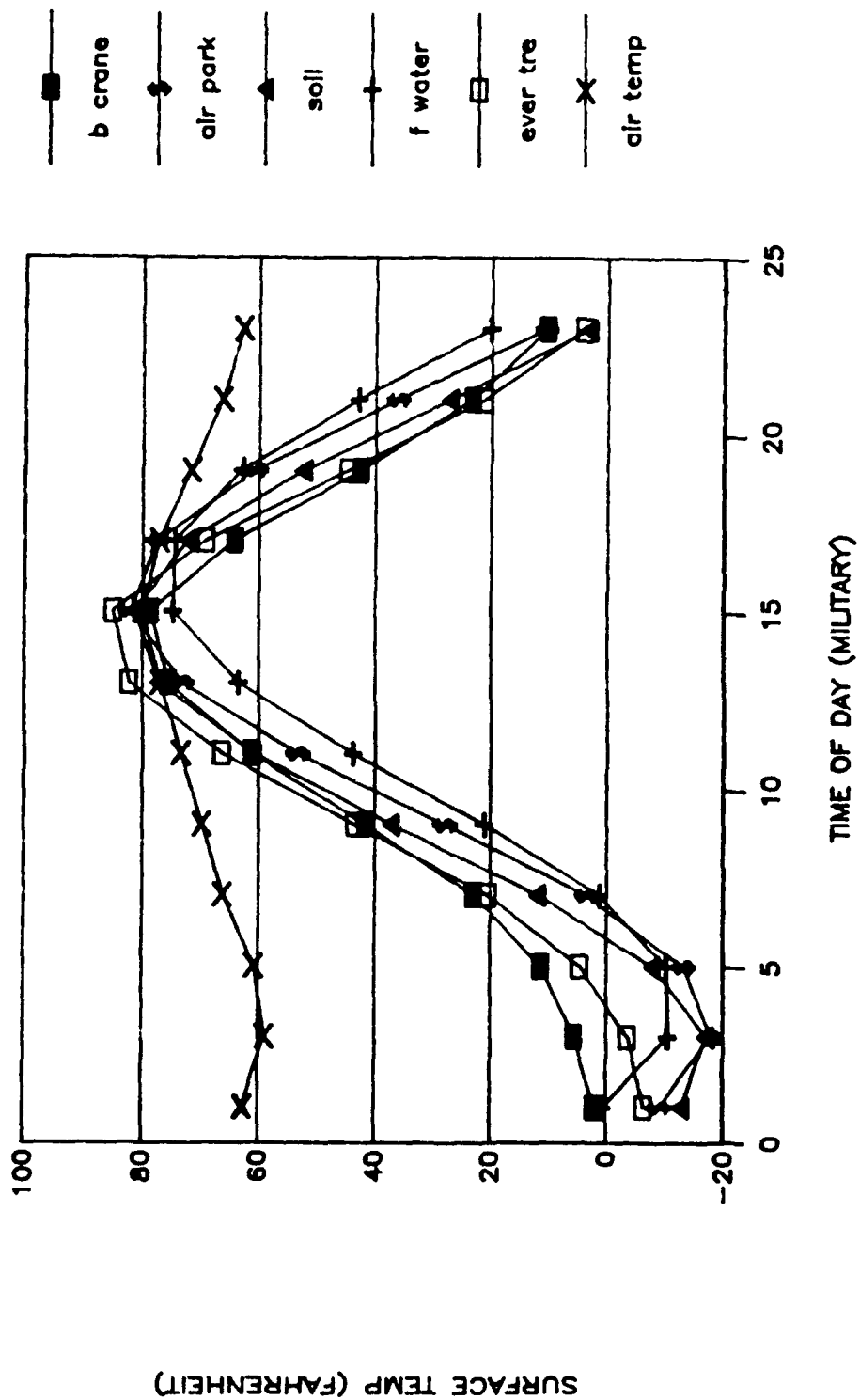


Figure 12. Phasor Solution for Capacitance Model.

Table 2. Sample Feature Magnitude and Phasor Coefficients

	<u>Bridge crane</u>	<u>Aircraft parking</u>	<u>Soil</u>	<u>Water</u>	<u>Evergreen tree</u>
Magnitude (R) °Fahrenheit	air temp.	82.1	81.4	76.1	70 °F*
Phase (θ_1)	.27°	19.7°	9.2°	29.3°	.48°

*Approximately the average of large feature magnitudes with the value of air temperature--in this instance 70 °F.

For both small and massive features, the estimated magnitudes in Table 2 are much too large. Recall that the results from Figure 12 and Table 2 indicate only the modulation of daily feature surface temperature around an average level which is denoted by Equation (16). Feature surface temperatures will not vary throughout a daily cycle by 100 °F (-20 °F from the average temperature at 2 a.m. and +80 °F at 2 p.m.). This shortcoming in the circuit model has pervaded all of our analyses. Only by including more resistance in the circuit or decreasing the modulation in the daily irradiance from the sun and sky can this problem be rectified.

Phase angles or the lag in heat accumulation by the features is also problematic, as shown in Figure 12 and Table 2. Table 2 shows that water heats and cools more slowly, followed by the aircraft parking area, soil, and finally the 2 small features. These findings are, as discussed in the previous section, directly related to the estimated capacitance for these features as shown in Table 1. For small features, the lag is approximately zero because their conductances, h_k (see Table 1), are large relative to all other factors in the denominator of the phase angle calculation (see Equation (18)). Of course, these conductance values are linearly related to d , the estimated feature thickness (i.e., $h_k = 2k/d$), and so would be quite sensitive to any changes in estimated feature thickness.

The revised capacity model in this section provided a better mechanism for allowing heat to be stored and released from individual features over time. Individual feature material parameters (e.g., feature thickness) and the circuit representation, however, are still problematic, preventing the model from producing reasonable surface temperatures across a daily cycle.

CONCLUSIONS

Heat transfer between media is a complex process. The idiosyncratic nature of the process makes it difficult to develop a general model for predicting feature surface temperatures as a function of environmental, geographic, temporal, and feature material input.

In the current IR predictive model in use at AL/HRA, shortcomings in a steady-state thermal predictive model led to large inaccuracies in predicting feature surface temperature for database features such as soil. Factors such as type of material, feature thickness, the attachment of a feature to a base of support, and the extent of the support are critical to predicting heat transfer and, consequently, feature surface temperature. Representing the continuous process of heat transfer in three-dimensional space by resistors, capacitors, and current and voltage sources in an electrical circuit necessarily involves simplification of the heat transfer process and the model suffers in the simplification process as discussed throughout this report.

Inclusion of heat capacity or the ability to store heat had no significant effect on softening extreme diurnal feature surface temperatures or providing a temperature lag throughout a diurnal cycle. Of course these findings are dependent upon the mathematical representation of capacitance and simply infer that the model is inadequate. Development of a more valid capacitance structure, however, would have to be couched in the circuit representation and, from the present analyses, it is evident that a more complex circuit representation is required.

The extreme feature surface temperatures across a daily cycle found in this report and previous reports may be alleviated by either--(a) adding more resistive elements in parallel with the current circuitry of the model which help to drain irradiance from the sun and sky, or (b) filtering the irradiance from the sun and sky to decrease the total amount of input flux to the circuit.

The relative heating and cooling of individual features across a daily cycle may be represented by including capacitors in the circuit model. However, given these more complex circuit representations, the predictions from the circuit representation are still limited by the accuracy of individual material coefficients. For example, relative lag time in the heating and cooling of the sample features in this report are entirely predicted by the electrical circuit capacity parameters. The orderings of these individual capacitance parameters for sample features in this report, however, were not as intuitively expected (e.g., we would intuitively expect water to heat and cool more quickly than soil but their estimated capacitance parameters from this report contradict this expectation).

REFERENCES

- Evans, R.J., & Crane, P.M. (1990). Infrared scene generation characteristics: A simulated feature analysis (AFHRL-TR-90-39, AD-B146 635L). Williams AFB, AZ: Operations Training Division, Air Force Human Resources Laboratory.
- Suits, G.H. (1985). Natural sources. In W.L. Wolfe & G. Zissis (Eds.) The infrared handbook: Chapter 3. Ann Arbor, MI: The Environmental Research Institute of Michigan.